Catalysis Letters Vol. 109, Nos. 3–4, July 2006 (© 2006)
DOI: 10.1007/s10562-006-0081-3

Characterization of iridium catalyst for decomposition of hydrazine hydrate for hydrogen generation

Sung June Cho,[a,*] Jun Lee,[a] Yun Sung Lee,[a] and Dong Pyo Kim[b]

[a]*Department of Applied Chemical Engineering and the Research Institute for Catalysis, Chonnam National University, Yong Bong 300, Buk-gu, Gwang-ju 500-757, Korea*

[b]*Department of Fine Chemical Engineering & Chemistry, Polymer-derived Advanced Ceramic Materials Laboratory, Chungnam National University, 220 Kung-dong, Yuseong-gu, Daejon 305-764, Korea*

Received 31 January 2006; accepted 23 March 2006

A catalyst with an ultra high iridium load was prepared using a method involving multiple impregnations. The obtained iridium catalyst contained between 29 and 35 wt% of 2 nm-sized nanoparticles dispersed on a support such as reinforced alumina, bauxite and precipitated alumina. XAFS suggested a possible structural model of Ir_4 surrounded by oxygen. The decomposition of hydrazine hydrate to its elements was used as a probe reaction. The results showed that a catalyst support with a high mechanical strength such as reinforced alumina and bauxite is essential for sustaining the decomposition reaction of hydrazine hydrate where there is a high degree of mechanical and thermal shock. The decomposition reaction of hydrazine monohydrate ($N_2H_4 \cdot H_2O$) proceeded rapidly to generate a CO_x-free hydrogen-rich gas through contact with the iridium catalyst at room temperature.

KEY WORDS: iridium catalyst; hydrazine hydrate; hydrogen generation.

1. Introduction

There has been considerable interest in hydrogen storage in addition to the transport technology for its utilization. Potential solutions using novel nanomaterials have been proposed and investigated extensively. Carbon adsorption using carbon nanotubes or modified carbon materials, metal borohydride technology based on the coupled recycling of $NaBH_4$–$NaBO_2$ and the Mg–MgO reaction etc. are promising technologies. However, many problems need to be overcome before they can be commercialized such as a high storage quantity, cost-effectiveness, etc. [1].

The decomposition of ammonia using a catalyst has been examined as a means of supplying CO_x-free hydrogen, which requires a high reaction temperature (>573 K) to be converted into nitrogen and hydrogen [2]. Hydrazine, N_2H_4, as monopropellant was investigated for use in satellite propulsion using an Ir based catalyst [3]. Shell405^{TM} (30 wt% Ir/Al_2O_3) was milestone in the development of such a catalyst, which activated anhydrous hydrazine even at 293 K [4]. Hydrazine can be converted in the following two ways: $N_2H_4(g) \rightarrow N_2(g) + 2H_2(g)$, $\Delta H = -95.4$ kJ mol^{-1} and $3N_2H_4(g) \rightarrow 4NH_3 + N_2(g)$, $\Delta H = -157$ kJ mol^{-1} [5].

Thus, the hydrazine can be used as a hydrogen source because it contains 12.5 wt% H, surpassing the DOE (Department of Energy, USA) target of 6.5 wt% H [6]. However, anhydrous hydrazine, $>98\%$ is highly toxic and explosive when exposed to a metal catalyst, making it difficult to apply safely. Hydrazine monohydrate, $N_2H_4 \cdot H_2O$, which also contains a large amount of hydrogen, 7.9 wt% H, is believed to be relatively safe. The further blending with water to 60% produces a hydrazine compound containing 4.7 wt% H, which is non-explosive [3]. In addition, the addition of water decreases and increases the melting and boiling points to 200 and 387 K, respectively, which can allow broader storage applications. Until now, hydrazine monohydrate has been used extensively as a foaming agent, anticorrosive agent, synthetic and chemical resin, rubber additive, pharmaceuticals, agricultural chemicals etc.

Therefore, hydrazine monohydrate might be a promising hydrogen carrier for storage and transfer. In this study, the preparation and characterization of a 30 wt% Ir catalyst on various supports was examined using X-ray diffraction, transmission electron microscopy, hydrogen chemisorption and X-ray absorption fine structure analysis. The catalytic activity of the Ir catalyst in decomposing hydrazine monohydrate ($>80\%$ purity) to its elements was measured.

2. Experimental

2.1. Preparation of iridium catalyst supported on various supports

$IrCl_3$ (54.26%, Johnson Matthey) was dissolved in 80 ml of water at room temperature and aged for 48 h. A set amount of the catalyst support was added to the

*To whom correspondence should be addressed.
E-mail: sjcho@chonnam.ac.kr

solution and stirred for 20 min. The wet catalyst support was dried with hot air for 5 min and heated at 653 K for 15 min to remove the acidic fumes. This wetting procedure was repeated to obtain the desired iridium content. After six repetition procedures, the sample was dried at 573 K for 1 h with flowing nitrogen and subsequently reduced with a hydrogen and nitrogen mixture (10:1) at 573 K for 30 min. This intermittent drying and reduction was essential to remove the acid accumulated on the catalyst. After the final impregnation, the sample was reduced with hydrogen at 823 K for 2 h. The reinforced alumina was purchased from Alcoa Co. The calcined bauxite was provided by Porocel Co. The precipitated alumina was made into a spherical shape through a precipitation method using ammonia. The samples were designated, Ir–R, Ir–B and Ir–P catalysts depending on the type of aluminas, the reinforced alumina, the calcined alumina and the precipitated alumina, respectively.

2.2. Characterization of the iridium catalyst

Hydrogen adsorption measurements were carried out at 298 K with a conventional volumetric gas adsorption apparatus according to the method described elsewhere [7]. The phase purity and the crystallinity of the sample was determined using powder X-ray diffraction (XRD, D/MAX Ultima III, Rikagu, Japan) with Cu $K\alpha$ radiation . The BET N_2 adsorption–desorption isotherms were measured at 77 K with ASAP2020 (Micromeritics, USA). The mechanical strength or crush strength of the catalyst support was measured using Desktop Instron (FGX-20R, SHIMPO Co., Japan). The maximum crush strength was measured by placing a particle of each catalyst on a stainless steel plate (t = 10 mm) under high pressure. The measurement was repeated 20 times the results are reported as an average.

Scanning electron micrographs were obtained using HITACHI S-4700 (Hitachi, Japan) operating at 25 kV. Elemental analysis was performed using an energy dispersive X-ray microanalyzer (Oxford, England) attached to the SEM. The transmission electron micrographs were taken using JEM2000FXII (Jeol, Japan) with an accelerating voltage of 200 kV.

X-ray absorption fine structure (XAFS) of the iridium catalyst was obtained under ambient conditions using *R*-XAS instrument (Rigaku, Japan) operating at 20 kV and 15 mA with a W filament, and also at Beamline 3C1 in the Pohang Accelerator Laboratory, Korea. The data was analyzed by the standard method using the *Ab initio* Feff program [8].

2.3. Catalytic activity test of decomposition of hydrazine monohydrate

The catalytic activity test of the catalyst in decomposing hydrazine monohydrate was performed in a batch reactor; a 150 ml three bottle-necked flask. Typically, 50 mg of catalyst was placed in the flask, which was then flushed with nitrogen for 20 min to remove the oxygen. One milliliter of hydrazine monohydrate (98%, Aldrich or 80% Yakuri Chemicals) was injected into the flask. The rate of gas evolution and the change in temperature was monitored using a MFM instrument (GFM17, Aalborg Co.) and the TPR (Hanyoung Co., Korea), respectively. The multiple reactions over the same catalyst were subsequently performed with an injection of hydrazine monohydrate after the each reaction was complete. The total amount of gas generation was calculated by integrating the gas evolution rate over a given time.

3. Results and discussion

Figure 1 shows the XRD patterns of the sample containing Ir on various supports. The XRD pattern showed only three major peaks at 40.5°, 46.8° and 68.7°2θ. These peak positions were assigned to Ir metal phase, which belongs to the *fm3m* space group with a = 0.384 nm. The peak position was slightly shifted to a lower angle by 0.2–0.5°, indicating lattice expansion in the Ir particles. The lattice spacing of the Ir particles obtained from the (111) peak was a = 0.385 nm. However, the large full width at half maximum (FWHM) suggested the formation of small Ir nanoparticles. The size of the Ir nanoparticle, which was estimated from the Scherrer equation assuming an instrumental line broadening factor of 0.115°, ranged from 1.5 to 1.8 nm [9], as shown in Table 1. Such a small particle generally displays lattice contraction [10]. The lattice expansion indicated from the XRD peak position is in contrast to the general phenomena observed for small metal particles.

It was also interesting that there was no typical alumina peaks, as shown in figure 1. The alumina generally showed the two relatively sharp peaks at 46.2° and 67.6° and one broad peak around 30–40°. The former peak splits into three peaks when the γ-Al_2O_3 is heated to

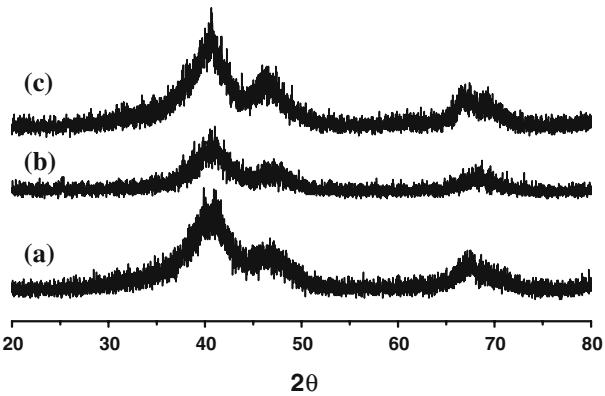

Figure 1. X-ray diffraction patterns of the (a) Ir–R catalyst, (b) Ir–B catalyst and (c) Ir–P catalyst.

Table 1
Nitrogen adsorption–desorption measurements at 77 K, hydrogen chemisorption at 298 K and particle size estimation

Sample	N_{imp}[a]	Wt%[b]	$S_{BET}(m^2g^{-1})$[c]	V_p, (cm^3g^{-1})[c]	$D_{H/Ir}$[d]	$d_{H/Ir}$(nm)[e]	d_{XRD}(nm)[f]
			185	0.369			1.7
Ir–R	18	35.4			0.37	2.7	
			(80)[g]	(0.278)[g]			(23.9)[g]
Ir–B	15	28.8	146	0.173	0.37	2.7	1.5
Ir–P	30	28.9	185	0.440	0.48	2.1	1.8

[a]Number of impregnations.
[b]weight percent according to EDX.
[c]Both are the surface area and pore volume, respectively.
[d]Dispersion based on the irreversible hydrogen chemisorption obtained from the difference between the total hydrogen chemisorption and the reversible hydrogen chemisorption at 298 K.
[e]Particle diameter estimated using $d_{H/Ir} = 1/(D_{H/Ir})$.
[f]Particle size estimated from the Scherrer equation using (111) peak at $2\theta = 40.5°$.
[g]after heating at 1173 K in hydrogen for 6 h.

1173 K. The absence of the Al_2O_3 phase was probably due to all the surface of the alumina being covered with Ir particles. The Ir–R catalyst showed the typical characteristic peaks corresponding to Ir metal when heated to 1173 K in hydrogen, as shown in figure 2. The surface area and pore volume of the catalyst was 80 $m^2\ g^{-1}$ and 0.273 $cm^3\ g^{-1}$, respectively, which suggested that the catalyst contained a large catalytically active surface area. However, Ir, IrO_2 and α-Al_2O_3 phases were observed when the sample was heated to 1373 K in air. The Ir to IrO_2 ratio obtained from the ICDD database was 55:45. In addition, the BET surface area obtained from the nitrogen adsorption isotherm was 5.0 $m^2\ g^{-1}$, indicating no catalytically active sites. This suggests that the mobility of the Ir nanoparticles increases when they are subject to oxygen, as has been reported with Ru nanoparticles [11]. However, it is unclear if the γ-Al_2O_3 to α-Al_2O_3 phase transformation in the Ir–R catalyst occurred at 1173 K under hydrogen. The phase transformation of the bare alumina used in the Ir–R catalyst, to α-Al_2O_3 occurred at around 1273 K with a large decrease in surface area to 60.3 $m^2\ g^{-1}$. The change in the surface area might depend on the presence of additives as well as on the preparation conditions of the support [12].

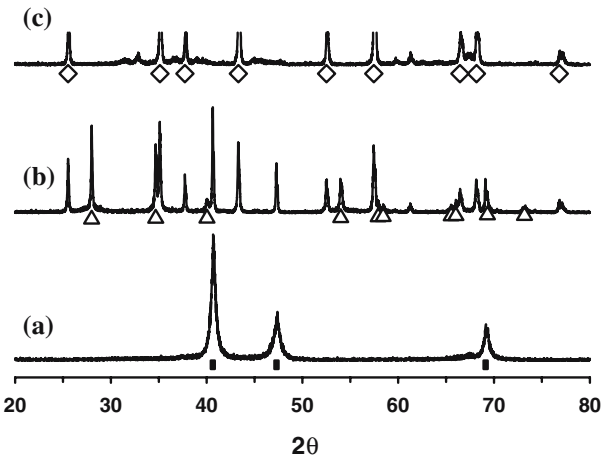

Figure 2. X-ray diffraction patterns of the (a) Ir–R catalyst heated in hydrogen at 1173 K, (b) Ir–R catalyst and (c) the bare alumina support heated in ambient air at 1373 K: (|) Ir metal, (Δ) IrO_2 and (◇) α-Al_2O_3.

The surface properties and particle size of the Ir catalyst was slightly affected. In particular, the particle size depends on the number of impregnations and the pore volume. A major component of bauxite is $Al(OH)_3$ with 5–10% SiO_2 and TiO_2 depending on the source. The calcined bauxite contained mostly alumina, γ-Al_2O_3. Increasing the number of impregnations might affect the size and distribution of the Ir nanoparticles, as shown in Table 1. A higher number of impregnations resulted in a smaller particle size. The Ir–P catalyst was supported on alumina, which was prepared by precipitation with ammonia. Therefore, it had a large surface area and pore volume, which was suitable for catalyst preparation. However, the low mechanical stability of the catalyst support might be an obstacle for the reaction when a high attrition loss is expected. Overall, hydrogen chemisorption on the Ir catalyst suggests that the multiple impregnations resulted in the formation of 2 nm sized Ir nanoparticle, irrespective of the catalyst support.

Figure 3 shows TEM images of the Ir–R catalyst. Under high magnification, it was found that the alumina surface was covered with Ir nanoparticles. The number average size of the iridium particles was 1.8 nm, which was consistent with the XRD and hydrogen chemisorption measurements. It should be noted that the separation between the iridium particles was almost the same as the dimensions of the particle size. Iridium particles might be susceptible to agglomeration due to the small separation. However, the agglomeration of the iridium particles was suppressed under a hydrogen atmosphere possibly due to the strong metal-support interaction, as shown in figure 2.

Figure 4 shows the Fourier transform of the Ir–R catalyst after a k^3-weighting of the XAFS spectrum, and its inverse Fourier transform between 0.149 and

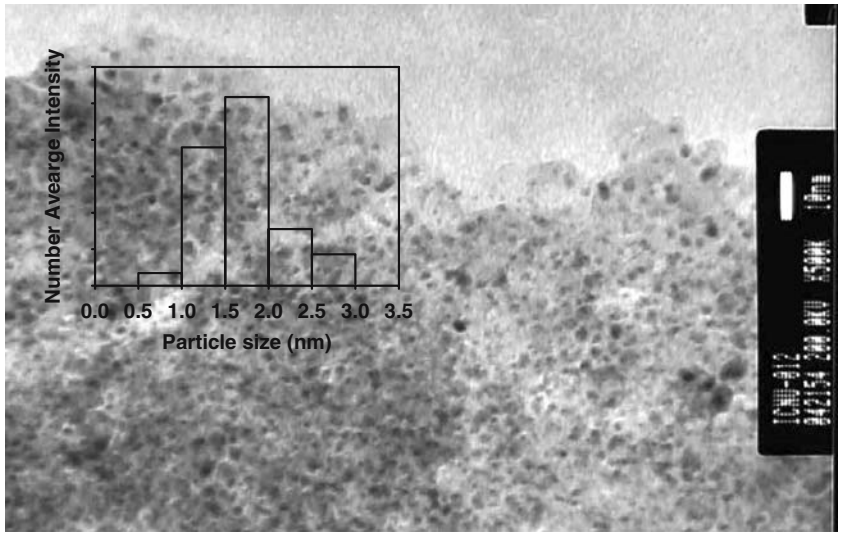

Figure 3. Transmission electron micrograph of the Ir–R catalyst. The inset shows the particle size distribution.

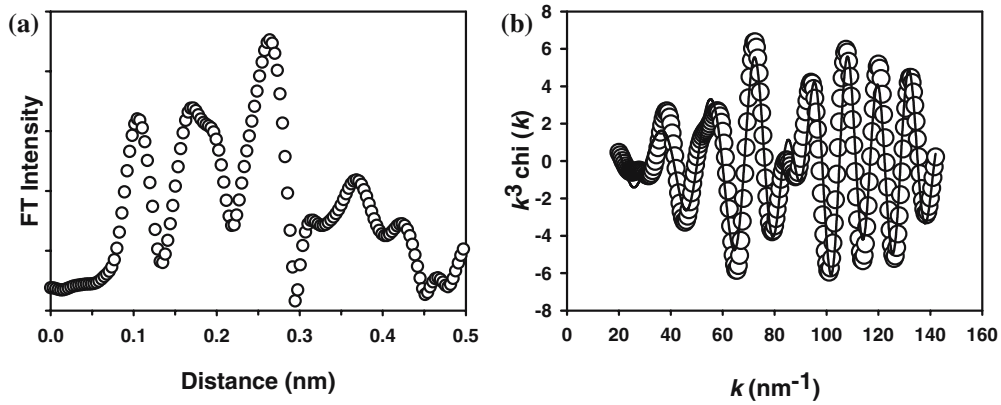

Figure 4. (a) Fourier transform after k^3-weighting of the XAFS oscillation and (b) its inverse Fourier transform between 0.149 and 0.308 nm. The solid line indicates the best curve fit.

0.308 nm. The XAFS data was analyzed using the UWXAFS2 program [13, 14]. The best curve fit preformed in *k*-space after the inverse Fourier transform is shown as a solid curve in figure 4(b). The obtained structural parameters are listed in Table 2. Two atomic pair distribution functions were obtained, an Ir–Ir pair at 0.271 nm and an Ir–O pair at 0.206 nm (figure 5). The coordination number (CN) suggested the presence of tetragonal Ir_4 with four to five oxygen atoms at the apex. The presence of the Ir_4 cluster in the supercage of the NaY zeolite and on the γ-Al_2O_3 was also confirmed by XAFS [15–17]. Such a small Ir_4 cluster was derived from the decarbonylation of the $Ir_4(CO)_{12}$ complex on the support. However, the Ir content was 1.0 wt%, which is extremely small compared with that prepared in this study. The possible structure was Ir_4O_x when the integer fitting was performed, where x = 10–14, as shown figure 6. The *R*-factor was minimized to 0.123 when the CN of the Ir–O pair was increased from 4 to 5. However, the structure contained the Ir–Ir distance, which is different from those in IrO_2, 0.315 and 0.355 nm. Rather, it was very similar to that of Ir metal, indicating an Ir metal structure surrounded by oxygen. Generally, the adsorption of oxygen can induce a relaxation of the distance [18]. The distance of the Ir–Ir pair is believed to be relaxed. Therefore, the relaxation of the bond distance of the Ir particle is consistent with the lattice expansion determined by XRD.

Figure 6 shows the change in the mechanical strength of the alumina against the heating temperature in ambient air. The precipitated alumina showed an inherent low mechanical stability (<10 lbs). The hydrazine decomposition reaction is highly exothermic with a large amount of thermal shock. Furthermore, the volume expansion due to the conversion of a liquid to nitrogen, hydrogen and ammonia gases will produce a high pressure inside the alumina pores. The Shell405^{TM} catalyst uses a unique high mechanical strength support, which was reported to be >17 lbs [4]. The reinforced alumina showed superior mechanical strength (50 lbs) at room temperature. The mechanical strength decreased progressively up to 1073 K and steeply to around 20 lbs

Table 2
Structural parameters obtained from EXAFS curve fitting for the Ir–R catalyst*

Pair	CN[a]	R (nm)[b]	σ^2 (pm^2)[c]	ΔE(eV)[d]	*R*-factor[e]
Ir–O	4.6	0.206	49	10.6 eV	0.121
Ir–Ir	2.7	0.271	18		

*Number of independent free parameters, N_{idp} and variable, N_{var} in the fit were 10 and 6, respectively, which was given by $N_{idp} = \frac{2\Delta k \cdot \Delta r}{\pi} + 2$, where Δk and Δr were 100 nm^{-1} (30–130 nm^{-1}) and 0.159 nm (0.149–0.308 nm, respectively).
[a]Coordination number (±0.5).
[b]Bond distance (±0.001 nm).
[c]the Debye–Waller factor.
[d]E_0 shift used in the fit.
[e]*R*-factor to measure the quality of the fit.

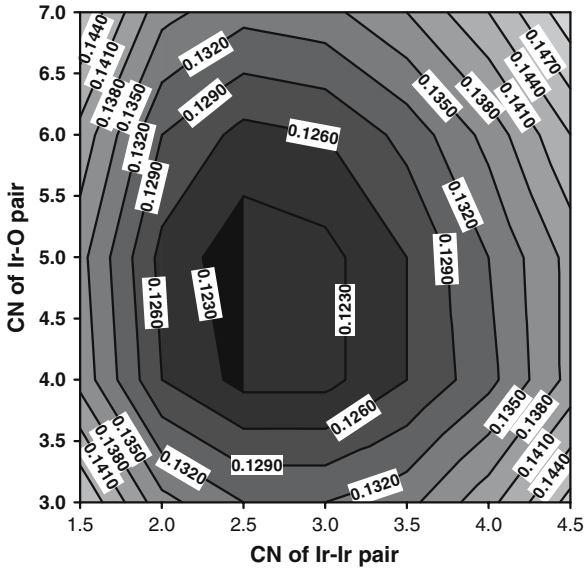

Figure 5. Contour map of the *R*-factor in the curve fit through integer fitting of the CN of the Ir–Ir and Ir–O pairs.

at above 1173 K due to the γ-Al_2O_3 to α-Al_2O_3 phase transformation. Calcined bauxite also had a much higher mechanical strength, 50 lbs at 1173 K. Such a high mechanical strength of the calcined bauxite was probably due to the presence of SiO_2 and TiO_2 as binders. It was reported that the SiO_2 binder retarded the sintering of the alumina, i.e. the increased phase transition temperature [12]. The phase transition of γ-Al_2O_3 plays a key role in decreasing the mechanical strength, the surface area etc. [19]. Therefore, only the Ir–R and Ir–B catalysts can be used for the decomposition of hydrazine hydrate where mechanical and thermal shock is large.

Figure 7 shows the rate of gas evolution and the change in temperature as a function of the reaction time during the decomposition of hydrazine monohydrate. Before the reaction, the reactor containing the Ir–R

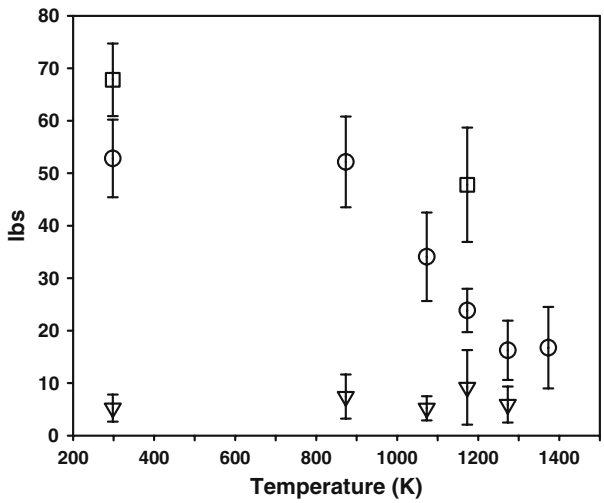

Figure 6. Crush strength of the bare alumina support against the heating temperature in ambient air: (○) the Ir–R catalyst; (□) the Ir–B catalyst; (▽) the Ir–P catalyst. The crush strength of 20 particles was measured.

catalyst (50.4 mg, 93 μmol Ir) was flushed with nitrogen to remove the oxygen. 1.0 ml hydrazine monohydrate (19.7 mmol, 98%) was then injected into the reactor. Initially, the rate of gas evolution was quite rapid; the reaction was complete within 1 min. In addition, the temperature increased to 340 K due to the exothermic reaction. Such a rapid reaction can also be due to the reaction between the product gas, hydrogen and the oxygen on the iridium nanoparticles, which would have reduced the iridium nanoparticles completely. It appears that the reduced state of the iridium nanoparticles remained for the subsequent reaction. The reaction time increased after five subsequent injections of hydrazine monohydrate. The catalyst particle remained the same under these reaction conditions. However, the particle size of the Ir–P catalyst decreased as a result of mechanical shock caused by the sudden generation of a large amount of gas inside the alumina pores.

The last two injections generated 2.40 *l* gas each with a reaction time of approximately 19.4 min, which was calculated from the integration of the gas evolution rate. This corresponded to 88.2 mmol gas when the temperature correction was carried out due to the heat released from the reaction. Considering the decomposition of $3N_2H_4{\cdot}H_2O(l) \rightarrow 4(1-x)NH_3(g) + (1+2x)N_2(g) + 6xH_2(g) + 3H_2O(g)$, the maximum gas evolution would be 91.9 mmol; 50 vol% hydrogen gas if all the hydrazine hydrate was converted into nitrogen and hydrogen, i.e. $x = 1$. The turnover number for hydrogen formation in the last injection was 0.85 s^{-1} based on all the Ir metal contained in the catalyst. The minimum gas evolution would be 52.5 mmol if all the hydrazine hydrate was converted to nitrogen and ammonia, i.e. $x = 0$. The reaction data is consistent with the almost complete conversion of hydrazine hydrate (>91%) into nitrogen

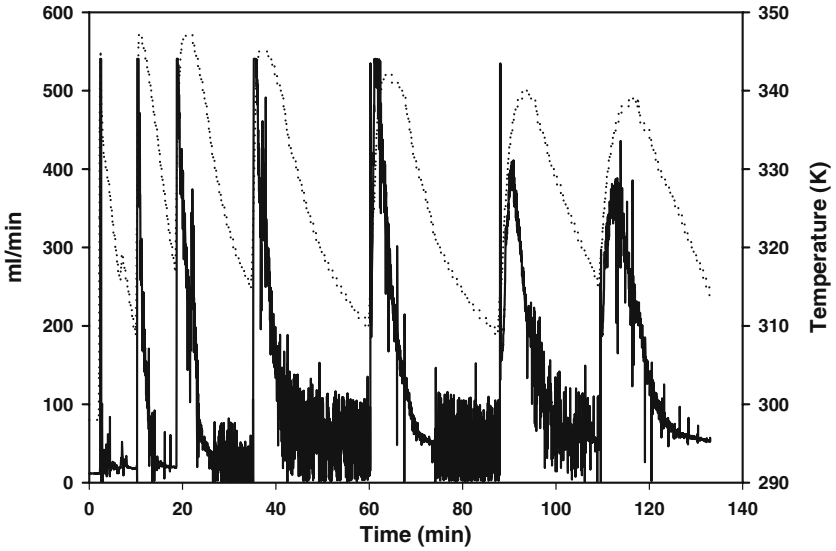

Figure 7. Gas evolution rate and temperature change against the reaction time during the decomposition of hydrazine hydrate. The solid line and dashed lines represent the gas evolution rate and temperature, respectively. Each injection was carried out after the evolution of gas was >95% complete.

and hydrogen. Furthermore, ammonia can also be converted into nitrogen and hydrogen at higher temperatures (573 K) if it formed during the decomposition reaction. The decomposition reaction of lower purity hydrazine hydrate such as 80% also occurred quite readily, suggesting the high activity of the Ir–R catalyst. The Ir–B catalyst also showed a similar catalytic performance.

4. Conclusion

An Ir catalyst was prepared through multiple impregnations of high mechanical strength alumina such as the reinforced alumina and the calcined bauxite into an Ir containing solution. The decomposition of hydrazine monohydrate over the Ir catalyst at room temperature resulted in the formation of mainly nitrogen and hydrogen. The ammonia can also be converted into nitrogen and ammonia at high temperatures using the same catalyst if it formed during the reaction. Therefore, a two-stage reformer can be designed to provide a CO_x-free hydrogen-rich gas to a fuel cell system: the first reactor converts hydrazine hydrate into nitrogen and hydrogen and the second reactor transforms ammonia into hydrogen and nitrogen at 573 K. Further study on the details of the catalytic reaction is currently underway.

Acknowledgments

This work was supported by Korean Research Foundation Grant (KRF-2003-003-D00087). The author (SJC) thanks the Pohang Accelerator Laboratory for the use of the Beamline 3C1 for the XAFS experiment.

References

[1] (a) E. Ewald, Int. J. Hydrogen Energy 23 (1998) 803; (b) H. Buchner, et al., *Hydrogen and other Alternative Fuels for Air and Ground Transportation* (Wiley, Chichester, UK, 1995).
[2] G. Papapolymerou and V. Bontozoglou, J. Mol. Catal. A 120 (1997) 165.
[3] E.W. Schmidt, *Hydrazine and its Derivatives: Preparation, Properties, Applications* (Wiley-Interscience, New York, 1984).
[4] W.E. Armstrong, L.B. Ryland and H.H.Voge, US Patent 4 (1978) 124,538.
[5] J.B.O. Santos, G.P. Valenca and J.A.J. Rodrigues, J. Catal. 210 (2002) 1.
[6] (a) *A National Vision of America's Transition to a Hydrogen Economy to 2030 and Beyond*, Department of Energy, USA, February (2002); (b) *National Hydrogen Energy Roadamp*, Department of Energy, USA, November (2002).
[7] (a) S.J. Cho, W.S. Ahn, S.B. Hong and R. Ryoo, J. Phys. Chem. 100 (1996) 4996; (b) R. Ryoo, S.J. Cho, C. Pak and J.Y. Lee, Catal. Lett. 20 (1993) 107.
[8] J.J. Rehr, R.C. Albers and S.I. Zabinsky, Phys. Rev. Lett. 69 (1992) 3397.
[9] (a) P. Scherrer, Nachr. Ges. Wiss. Gottigen, Math-Phys. Kl. 2 (1918) 96; (b) R. Jenkins and R.L. Snyder, *Introduction to X-ray Powder Diffractometry* (Jonn Wiley & Sons, New York, 1996).
[10] D.C. Koningsberger and B.C. Gates, Catal. Lett. 14 (1992) 271, and reference therein.
[11] S.J. Cho, J.E. Yie and R. Ryoo, Catal. Lett. 71 (2001) 163.
[12] (a) M.H. Han, Y.S. Ahn, S.K. Kim, S.K. Shon, S.K. Kang and S.J. Cho, Mat. Sci. Eng. A 302 (2001) 286; (b) R.M. German, *Sintering Theory and Practice* (John Wiley & Sons, INC., New York, 1996).
[13] E.A. Stern, M. Newville, B. Ravel, Y. Yacoby and D. Haskel, Physica B 208 (1995) 117.
[14] M. Newville, P. Livins, Y. Yacoby, J.J. Rehr and E.A. Stern, Phys. Rev. B 47 (1993) 14126.

[15] A.M. Argo and B.C. Gates, Langmuir 18 (2002) 2152.
[16] F. Li and B.C. Gates, J. Phys. Chem. B 108 (2004) 11259.
[17] A.M. Argo, J.F. Odzak and B.C. Gates, J. Am. Chem. Soc. 125 (2003) 7109.
[18] E.J. Inglesfield, Progr. Surf. Sci. 20 (1985) 105.
[19] S.J. Cho, Y.S. Seo, K.S. Song, N.J. Jeong and S.K. Kang, Appl. Catal. B: Environ 30 (2001) 351.